Estimation of Daily Winter Precipitation in the Snowy Mountains of Southeastern Australia

JINGRU DAI, MICHAEL J. MANTON, AND STEVEN T. SIEMS

School of Mathematical Sciences, Monash University, Clayton, Victoria, Australia

ELIZABETH E. EBERT

Centre for Australian Weather and Climate Research, Melbourne, Victoria, Australia

(Manuscript received 14 May 2013, in final form 20 September 2013)

ABSTRACT

Wintertime precipitation in the Snowy Mountains provides water for agriculture, industry, and domestic use in inland southeastern Australia. Unlike most of Australia, much of this precipitation falls as snow, and it is recorded by a private network of heated tipping-bucket gauges. These observations are used in the present study to assess the accuracy of a poor man's ensemble (PME) prediction of precipitation in the Snowy Mountains based on seven numerical weather prediction models. While the PME performs quite well, there is significant underestimation of precipitation intensity. It is shown that indicators of the synoptic environment can be used to improve the PME estimates of precipitation. Four synoptic regimes associated with different precipitation classes are identified from upper-air data. The reliability of the PME forecasts can be sharpened by considering the precipitation in each of the four synoptic classes. A linear regression, based on the synoptic classification and the PME estimate, is used to reduce the forecast errors. The potential to extend the method for forecasting purposes is discussed.

1. Introduction

The Snowy Mountains of southeastern Australia are the source of much of the water used for irrigation, industry, and domestic use along the Murray and Murrumbidgee Rivers of inland Australia. These mountains rise up to 2000 m, with winter snow making a significant contribution to the annual river runoff in this region. Since snow is uncommon in Australia, the difficulties in observing and predicting it have generally been avoided. Larsen and Nicholls (2009) find that cool season precipitation in southern Australia is related to the intensity and position of the subtropical ridge. Timbal and Drosdowsky (2013) show that strengthening of the subtropical ridge contributed to the major droughts of 1935–45 and 1997–2009. Chubb et al. (2011) develops a climatology and airmass history for winter precipitation in the Snowy Mountains and attributes an observed decline in winter precipitation to changes in the frequency and intensity of cold fronts. Further research shows the rainfall decline to be also linked to trends in the southern annular mode (SAM; Nicholls 2010). Modeling by Kent et al. (2013) suggests that changes in the subtropical ridge may be associated with changes in the global meridional circulation, which in turn are linked to global climate change.

While there is a growing understanding of the large-scale factors affecting the climate of the Snowy Mountains, the forecasting of daily precipitation remains a continuing challenge for the region, with difficulties arising from the measurement of snow in windy conditions and from the impacts of the local orography on the spatial variability of precipitation. Simulating precipitation in this region may be even more difficult given the frequent observations (up to 40% of wintertime) of supercooled liquid water during the winter months (Morrison et al. 2013). Recently, Chubb et al. (2012), examined wintertime case studies of precipitation events in the nearby Brindabella Ranges, highlighting the extended periods of postfrontal precipitation that correspond to the time of supercooled liquid water being observed.

The Australian Bureau of Meteorology (BoM) runs a routine rainfall prediction scheme for Australia based on a poor man's ensemble (PME) of the output of seven

Corresponding author address: Jingru Dai, School of Mathematical Sciences, Monash University, Clayton, VIC 3800, Australia.
E-mail: jingru.dai@monash.edu

DOI: 10.1175/JHM-D-13-081.1

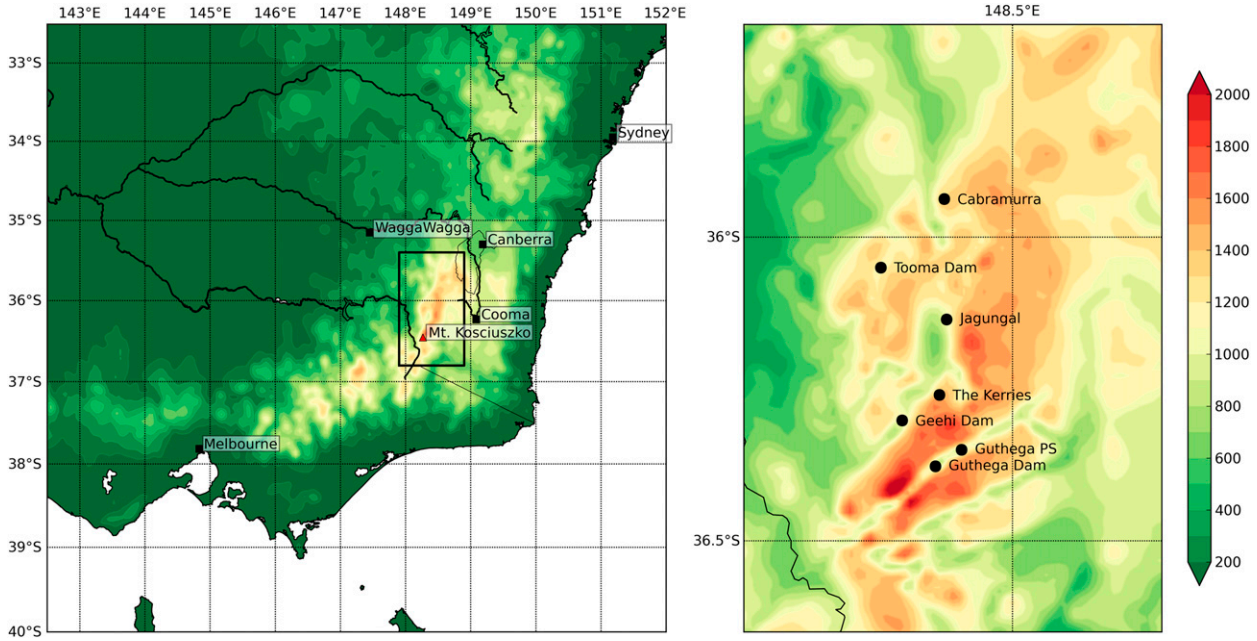

FIG. 1. Snowy Mountains region in southeastern Australia and rain gauges used in this study.

different numerical weather prediction models (Ebert 2001). Across Australia the forecasts are found to be consistent and accurate (further information is available at http://www.bom.gov.au/watl/about/rainfall-forecast-review.shtml).

The PME forecasts are generated and evaluated on a 1° latitude–longitude grid. They predict precipitation probability and amount, but this study only considers rainfall amount. Johnson et al. (2013) compared PME forecasts against observations from the Australian Water Availability Project (AWAP; Raupach et al. 2008) and found that wintertime PME precipitation forecasts performed relatively poorly over the Snowy Mountains in comparison to nonorographic or noncoastal grids across the southern portion of Australia. Because the rain gauges at high elevation used in this study are operated by Snowy Hydro Ltd., they are not available to the AWAP dataset or the routine BoM observation network; thus, a larger bias than in Johnson et al. (2013) from PME can be expected. Therefore, more detailed information will be obtained by considering their behavior over the relatively small area of the Snowy Mountains (Fig. 1). In particular, a statistical technique is used in this study to determine whether the performance of the PME can be improved by adjusting the PME value by a factor that depends upon the large-scale environment. The nature of the large-scale environment is estimated from sounding data observed at Wagga Wagga, 180 km to the west of the Snowy Mountains.

There has been a considerable amount of work on quantitative precipitation forecasting and the application of downscaling methods to adjust the output of numerical models (Abaurrea and Asín 2005; Bergant and Kajfež-Bogataj 2005; Fowler et al. 2007). Model output statistics (MOS) is an objective forecasting technique that makes use of the statistical relationship between model output and observed local weather variables (Glahn and Lowry 1972). The primary advantage of MOS is that model biases and local climatology are automatically built into the equations (Klein and Glahn 1974; Brunet et al. 1988). The classical approach to quantitative precipitation forecasting (Lorenz 1969) is analog based, where one or more specific predictors (e.g., mean sea level pressure) are used to estimate a site-specific parameter (e.g., precipitation). A statistical relationship is built between local observations and large-scale model output variables, under the assumption that these relationships will persist outside the training period (the period where observations or reanalysis data were used to define the relationship between large-scale model outputs and local meteorology).

Enke and Spekat (1997) apply a cluster analysis to a set of upper-air observations to characterize the weather regime for a European area. A stepwise screening regression analysis is then carried out for each surface weather element to be predicted. They find that the approach is effective for downscaling daily output from a global climate model in terms of explained variance for temperature, but it is less useful for precipitation. It is

TABLE 1. Sites of precipitation gauges in the Snowy Mountains, establishment dates, and mean winter (May–October) precipitation.

Site	Lon (°)	Lat (°)	Elev (m)	Start year	Mean winter precipitation (mm)
Cabramurra	148.38	−35.94	1482	1955	707
Geehi Dam	148.31	−36.30	1175	1992	1082
Guthega Dam	148.37	−36.38	1558	1994	884
Guthega Power Station	148.41	−36.35	1320	1994	932
Jagungal	148.39	−36.14	1659	1990	1157
The Kerries	148.38	−36.26	1740	1995	832
Tooma Dam	148.28	−36.05	1221	1992	1130

found that the probability of precipitation (POP) and the precipitation amount in alpine areas both have 15%–25% of explained variance, compared with about 80% for temperature.

In the present work, where the basic prediction comes from an ensemble of models, we use only observed data to adjust the PME forecast. This approach means that the system does not depend upon the performance of an individual model (as arises with most downscaling methods), and so it should provide a robust adjustment to the PME forecasts, which have been shown to have good overall performance (Ebert 2001). The approach uses the sounding data from Wagga Wagga to assign a class to the daily synoptic weather features, and the adjustment to the PME forecast varies with the synoptic class.

2. Datasets

The basic dataset for this study is the daily precipitation measured at seven sites above 1100 m across the peaks of the Snowy Mountains (Fig. 1) over the 20-yr period from 1990 to 2009. These sites, which are representative of the higher ranges, are part of a network operated by Snowy Hydro Ltd. that was established over the early 1990s. Table 1 shows the location and establishment date for each of the precipitation gauges, which use well-maintained heated tipping buckets. The gauge data are quality controlled and archived as hourly records, which are aggregated to yield daily precipitation values at 0900 local time (LT) to align with the conventional observation time for daily precipitation by the BoM. While heated tipping buckets are not the most sophisticated technology for the measurement of solid precipitation, the network of seven gauges does provide a homogeneous 20-yr record with precipitation values consistently greater than those observed at lower elevations.

Chubb et al. (2011) show that the precipitation for these high-elevation sites has monthly values of around 200 mm from June to September, which are almost double the amount compared with low-elevation sites on the slopes, and that most of the precipitation in the winter period of May–October is associated with the passage of cold fronts. We also see from Table 1 that the winter precipitation is fairly uniform across these sites, and so we take the daily-mean value as the core variable for the present analysis.

Basic prediction of the daily precipitation is obtained from the PME forecasts provided by the BoM (Ebert 2001) on a 1° grid across Australia. The mean value of the four closest grid points is taken as the PME estimate of the precipitation across the region of interest. Forecasts are provided up to 72 h ahead, and so we consider each of the three 24-h periods as separate estimates of precipitation on a given day. Although the individual models and the PME system itself evolve with time, a relatively consistent time series of PME forecasts is available for the period 2005–09.

The closest upper-wind site of the BoM to the Snowy Mountains is Wagga Wagga (Fig. 1), which lies 180 km to the northwest. The appropriateness of this site is indicated by Chubb et al. (2011), who show that moisture during winter precipitation events commonly reaches the Snowy Mountains from the northwest. Daily soundings are taken at 1000 LT in winter, and these data are used to provide an estimate of the large-scale environment of the weather affecting the Snowy Mountains. The sounding data are obtained from the University of Wyoming (http://weather.uwyo.edu/upperair/sounding.html), and 3153 days of valid data are found for the period 1990–2009.

Using the standard-level data from the soundings, daily values of the following six basic variables are computed to represent the large-scale environment:

- root-mean-square (RMS) wind shear between 850 and 500 hPa (SH),
- total totals index (TT),
- westerly moisture flux up to 250 hPa (QU),
- southerly moisture flux up to 250 hPa (QV),
- total moisture up to 250 hPa (TW), and
- surface pressure at Wagga Wagga (GP).

The correlations between these variables are not high, with a peak correlation of −0.49 between GP and QU, and so we treat them as independent measures of the large-scale environment. The variables SH and TT give a representation of the stability of the atmosphere, while QU, QV, and TW indicate the flux and amount of water available for the formation of precipitation. TT is defined as $T(850) - 2T(500) + T_d(850)$, where $T(x)$ is the temperature (°C) at pressure level x (hPa) and T_d is the dewpoint temperature (°C). It is recognized by forecasters

TABLE 2. Monthly-mean daily precipitation statistics for the Snowy Mountains over the period 1990–2009; quartiles apply to rain days (i.e., precipitation intensity).

Month	Frequency of daily precipitation	Q1 (mm)	Median (mm)	Q3 (mm)
May	0.37	6.3	7.2	12.1
Jun	0.56	8.3	12.2	15.9
Jul	0.58	8.2	9.6	12.0
Aug	0.59	9.8	11.6	13.7
Sep	0.54	10.2	12.8	14.9
Oct	0.46	7.9	9.4	14.0

as a simple measure of static atmospheric stability (e.g., Henry 2000). Changes in surface pressure can be effective predictors of precipitation (e.g., Fraedrich and Leslie 1987), and so GP is included in the analysis. Direct measures of the wind (such as the 850-hPa vector wind) are not included in the analysis, because such variables are highly correlated (about 0.8) with the moisture fluxes.

3. Characteristics of winter precipitation

Table 2 summarizes the statistics of precipitation in the Snowy Mountains in the wintertime (i.e., the 6 months of May–October 1990–2009, averaged over all seven sites). The resolution of the precipitation gauges is 0.25 mm, and so this value is taken as the threshold between rain and no-rain days. The frequency of daily precipitation (FOP) each month varies smoothly across wintertime, rising to a peak of about 0.6 in July and August. The median daily precipitation on rain days (intensity for rain days) for June–September is about 10 mm, with lower values in the transition months of May and October. The third quartile of precipitation is consistently around 14 mm across wintertime, with lower values in May and July.

The precipitation of southeastern Australia has high interannual variability; for example, the July mean-daily precipitation has varied from 2.5 mm in 1994 to 11 mm in 1995. The median rainfall at high elevation has a double-peaked structure in the 20-yr statistics. In fact, for this 20-yr period, half of the time July had more precipitation than June. However, the dry Julys in the early 1990s and early 2000s strongly influenced the overall statistics.

Precipitation in southeastern Australia is found to be affected by large-scale climate features in the Pacific and Indian Oceans and at high latitudes (e.g., Risbey et al. 2009). These features are represented by the Southern Oscillation index (SOI), the Dipole Mode Index (DMI; a measure of the Indian Ocean dipole; Saji and Yamagata 2003), and SAM. Smith and Timbal (2012) suggest that, while such indices appear to be linked to the precipitation of southeastern Australia on interannual time scales, long-term trends seem to be linked with changes in the large-scale atmospheric circulation related to mean sea level pressure. The monthly-mean precipitation in the Snowy Mountains is shown in Fig. 2, together with time series of DMI and GP. The correlation between monthly precipitation and the DMI is −0.26 at the 0.04% significance level, while the correlations with SAM and SOI are smaller and much less significant. The correlation with GP is −0.53 with a P value smaller than 10^{-9}. Thus, we find that precipitation in the Snowy Mountains has interannual variability consistent with that found across southeastern Australia.

Table 3 summarizes the performance of the PME forecasts over the period 2005–09. The analysis is separated into the FOP and the statistical characteristics on rain days. The observed FOP is computed using a threshold of 0.25 mm based on the characteristics of the observing system (Table 2). To ensure a comparable analysis of the PME data, we choose a forecast value threshold that yields a contingency table with a frequency bias score of 1.0 (Ebert 2001). In this way, we obtain a threshold that balances across the contingency table, that is, the number of misses and false alarms are the same, as are the number of rain days in the forecast and observations. Thus, the threshold for a rain day is 0.45 mm for the PME data. We see that the hit rate (or probability of detection) for rain days decreases from 0.79 on day 1 to 0.73 on day 3, and the RMS error on no-rain days (i.e., error in precipitation intensity) varies from 1.2 to 1.9 mm, with the smallest error on day 2. The false-alarm rate for no-rain days is around 0.2. The errors on rain days also tend to be smallest on day 2. The RMS error on rain days is around 11.5 mm. These RMS errors are much larger than those reported by Ebert (2001), but the latter were calculated over a much larger area. Moreover, the gauges used in the present study are not available for the routine PME analyses, and so it is likely that the relatively high rainfall of the Snowy Mountains is not well represented in the PME calibration process.

There is large interannual variability in both the basic rainfall statistics and the performance of the PME. In Table 4 we compare the rainfall statistics and PME performance for day-1 forecasts over the period 2005–09. It is seen that the rain-day hit rate varies from 0.86 in 2005, when the intensity was 10.9 mm, to 0.66 in 2006 (a year of major drought), when the intensity was 6 mm. The RMS errors for those years were 14 and 7 mm, respectively. Thus, there appears to be a relationship between PME performance and the overall rainfall for each year; for example, 2006 has the lowest annual

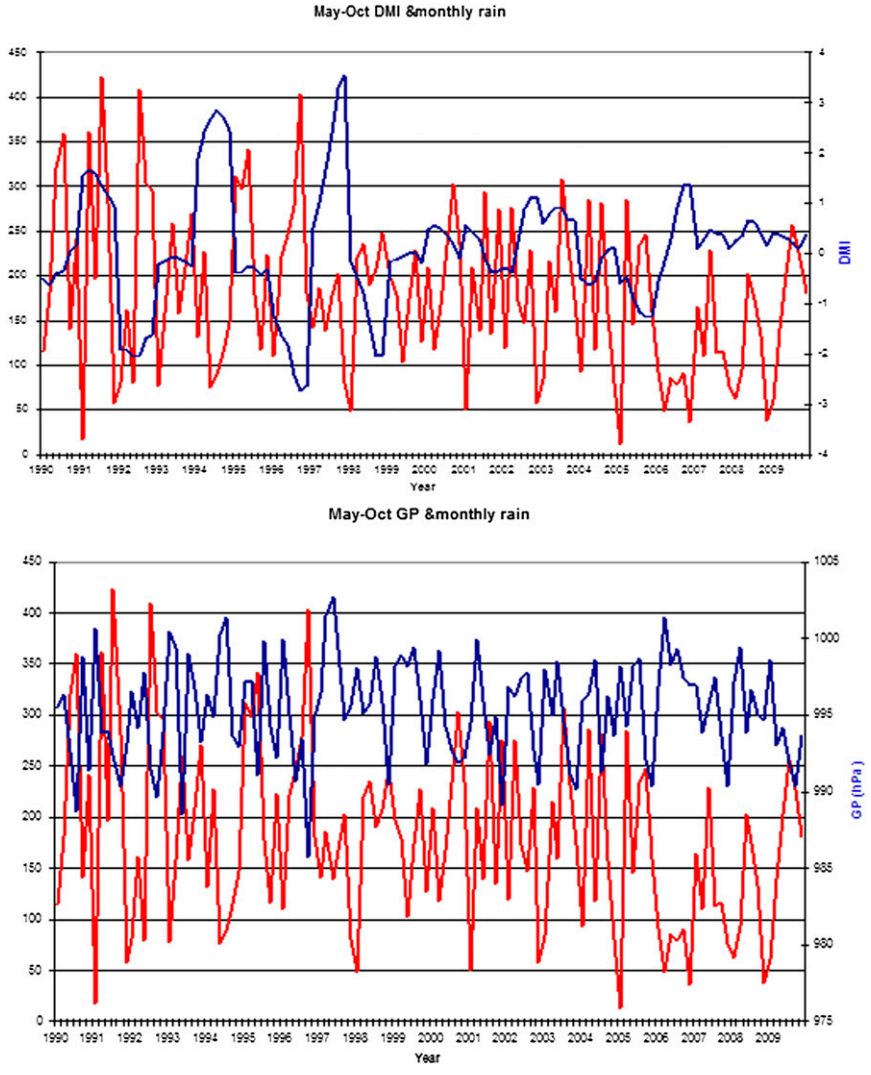

FIG. 2. Time series of monthly-mean precipitation in the Snowy Mountains (red), with time series (blue) of climate drivers (top) DMI and (bottom) GP.

rainfall for the period, and it has the lowest PME hit rate and rain-day errors. Because the PME uses probability matching for the ensemble mean of the individual model predictions (Ebert 2001), the method tends to perform better in heavy rainfall events. Moreover, light rainfall can be smoothed out over alpine regions where the number of available sites for creating the PME is limited.

While the performance of the PME varies with the wintertime rainfall, its performance on no-rain days has much less interannual variability. This behavior is expected as the criterion for a no-rain day is fixed. It is noted, however, that the false-alarm rate for no-rain days is very large in 2009; this may be associated with the high number of rain days (109) in that year. Although

TABLE 3. Basic performance of PME forecasts over the period 2005–09 for 1, 2, and 3 days ahead, using a threshold of 0.25 mm for observations and 0.45 mm for PME.

Forecast period	Rain-days hit rate	No-rain-days false-alarm rate	RMS error on rain days (mm)	Bias on rain days (mm)	RMS error on no-rain days (mm)	Bias on no-rain days (mm)
Day 1	0.79	0.21	11.5	5.16	1.59	0.47
Day 2	0.75	0.20	11.2	4.65	1.23	0.41
Day 3	0.73	0.24	11.6	4.70	1.94	0.65

TABLE 4. Interannual variability of rainfall observation and of PME performance for day-1 forecasts over period of 2005–09 winter.

Variable	2005	2006	2007	2008	2009
Total precipitation (mm) (obs)	1082	429	809	703	1067
No. of rain days (obs)	99	72	91	86	109
Rainfall intensity (mm) (obs)	10.9	6.0	8.9	8.2	9.8
PME rain-day hit rate	0.86	0.66	0.74	0.86	0.83
PME RMS error on rain days (mm)	13.85	7.05	10.06	10.48	13.96
PME bias on rain days (mm)	6.82	1.77	3.86	4.44	8.38
PME no-rain-day false-alarm rate	0.19	0.21	0.20	0.16	0.32
PME RMS error on no-rain days (mm)	1.92	1.71	1.22	1.33	1.45
PME bias on no-rain days (mm)	0.52	0.43	0.40	0.37	0.62

the operational PME system has evolved over its lifetime, we do not detect any significant trend or change in the performance of the system over the analysis period.

4. Synoptic classification

It has been shown that the classification of weather systems in southeastern Australia can be readily carried out through examination of synoptic mean sea level pressure charts (Pook et al. 2006; Chubb et al. 2011). Recently, Wilson et al. (2013) have used upper-air soundings at a single site to carry out a synoptic analysis for southeastern Queensland. This technique is applied to the present study. We use a *k*-means clustering algorithm (Hartigan and Wong 1979) to assign a synoptic class to the daily sounding from Wagga Wagga (Fig. 1). The six variables identified in section 2 are normalized to zero mean and one standard deviation and are then analyzed with the number of clusters varying from 2 to 5. As the variance between clusters tends to gradually decrease as the number of clusters is increased, it is often difficult to determine the optimal number of clusters for the *k*-means approach. However, for this study, the focus is on the use of the classification to distinguish different synoptic regimes associated with precipitation. We therefore increase the number of clusters only while each cluster has a unique observed precipitation distribution associated with it. That is, we calculate the distribution of daily precipitation associated with each cluster and then apply a Kolmogorov–Smirnov test (Marsaglia et al. 2003) to ensure that each distribution is distinct. Figure 3 shows that distinct rainfall distributions are obtained with four synoptic clusters. However, extending the number of clusters (or classes) to five does not lead to distinct precipitation distributions, so we focus on four classes for this analysis.

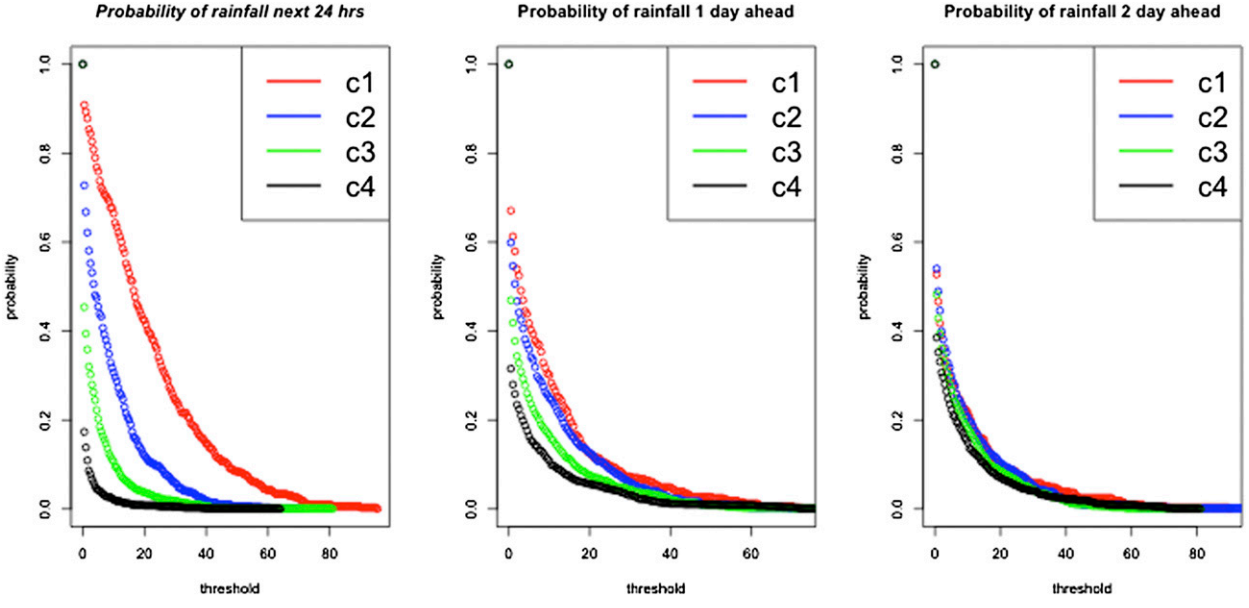

FIG. 3. Probability distribution of daily rainfall for four clusters: (from left to right) the daily rainfall for the next 24 h after sounding measurement, daily rainfall 1 day ahead, and daily rainfall 2 days ahead.

TABLE 5. Statistical properties of precipitation in each synoptic class from a four-cluster analysis. The first result is for a 20-yr period (1990–2009), and the second result is for a 5-yr period (2005–09).

Class	Frequency	POP	Mean intensity (mm)	Fraction of winter precipitation
C1	0.10, 0.09	0.92, 0.88	22.4, 20.0	0.40, 0.33
C2	0.21, 0.20	0.75, 0.68	10.9, 11.3	0.32, 0.33
C3	0.36, 0.39	0.50, 0.53	6.7, 6.5	0.22, 0.29
C4	0.33, 0.32	0.21, 0.26	4.0, 2.4	0.05, 0.05

One disadvantage of the present approach to classification is that the temporal and spatial resolution can be limited. The observed soundings only represent the vertical profile of the atmospheric condition at a certain time (in this case, 1000 LT each day) and place (in this case, 180 km to the northwest of the area of interest). On the other hand, substantial changes can occur in the structure of the atmosphere within hours and over small areas, for example, with the passage of a cold front. This resolution uncertainty can at least partly explain some of the variability in the precipitation distribution between synoptic classes. By moving the 24-h precipitation window and checking the Kolmogorov–Smirnov test significance, it is found that the use of the daily sounding to estimate the distribution of daily precipitation is best only for the following 24-h period. Figure 3 shows the probability distribution of 24-h precipitation for three 24-h periods: the period directly after the sounding, the period 1 day ahead, and the period 2 days ahead. It is seen that distinct probability distributions are not apparent at the longer time periods. While there is some distinction for 1 day ahead, by 2 days ahead, the precipitation distributions cannot be separated by synoptic class. In the present study, we therefore focus on the daily precipitation on the day of the sounding; that is, for upper-air variables taken at 1000 LT 1 May, the corresponding daily precipitation is measured at 0900 LT 2 May.

This restriction limits the capability of this approach for forecasting applications. It arises because the synoptic regime varies as precipitating systems move across the region. However, it may be possible to use a simulated sounding from a numerical weather prediction model to classify the synoptic situation some days ahead, and this aspect could be explored in a future study.

Table 5 summarizes the statistics of the precipitation for each class when a four-cluster analysis is applied to the six synoptic variables over the period 1990–2009. It is seen that there are two classes (C1 and C2) with high intensity (22 and 11 mm) but low frequency of occurrence (0.10 and 0.21), one (C3) with moderate intensity (7 mm) and moderate frequency (0.36), and one (C4) with lower intensity (4 mm) and slightly lower frequency (0.33). The POP decreases from 0.9 for C1 to 0.2 for C4. It is apparent that none of the synoptic classes can be considered to be completely dry, but C4 makes up only 5% of the total winter precipitation. On the other hand, C1 has a very high probability of high precipitation and makes up 40% of winter precipitation. C2, which has half the intensity of C1, makes up 32% of winter precipitation. The most frequent class is C3, which occurs 36% of the time and contributes 22% of the winter precipitation. The precipitation statistics for the period 2005–09 are also shown in Table 5. The cluster-based characteristics are unaffected in this shorter period, which is used to evaluate the PME forecast.

Figure 4 shows the (scaled) variables at the center of each synoptic class for the four-cluster analysis. The classes, which are initially ordered by decreasing POP, have increasing values of surface pressure (GP), with C1 having a median value of 989 hPa and C4 having 1001 hPa. The moisture flux for C1 is about 10 times greater than for C4; that is, the surface pressure and moisture fluxes clearly delineate the two extreme classes. Each class has a mean westerly component of the moisture flux. C1 and C3 have mean northerly components, while C2 and C4 have mean southerly components. This result is consistent with the observation of Chubb et al. (2011) that most of the precipitation in the Snowy Mountains tends to come from winter fronts propagating from the west with moisture trajectories from the northwest. On the other hand, there is considerable variability within each class. We note that C2 has the greatest mean shear and only a moderate moisture flux, which probably limits the precipitation intensity. The driest class (C4) has a moderate shear, but very low values of TT, total water, and moisture flux.

In summary, C1 is a very wet class with a very high northwesterly moisture flux, very high instability and total integrated water, and low surface pressure. It has a low frequency of occurrence (10%) but contributes 40% of winter precipitation. C2 is moderately wet with a moderate westerly flux, very high shear, and low surface pressure. It has a frequency of about 20% and contributes about 30% of winter precipitation. C3 is relatively dry with a low westerly moisture flux, high instability, and low shear. It occurs about 35% of the time and contributes about 25% of the winter precipitation. C4 is the driest class with a low southwesterly flux, low total water, and high stability. It occurs about 35% of the time and contributes only 5% of winter precipitation.

The seasonal variability of the frequency of each class is shown in Fig. 5. It is apparent that the two wettest classes (C1 and C2) occur more frequently toward the

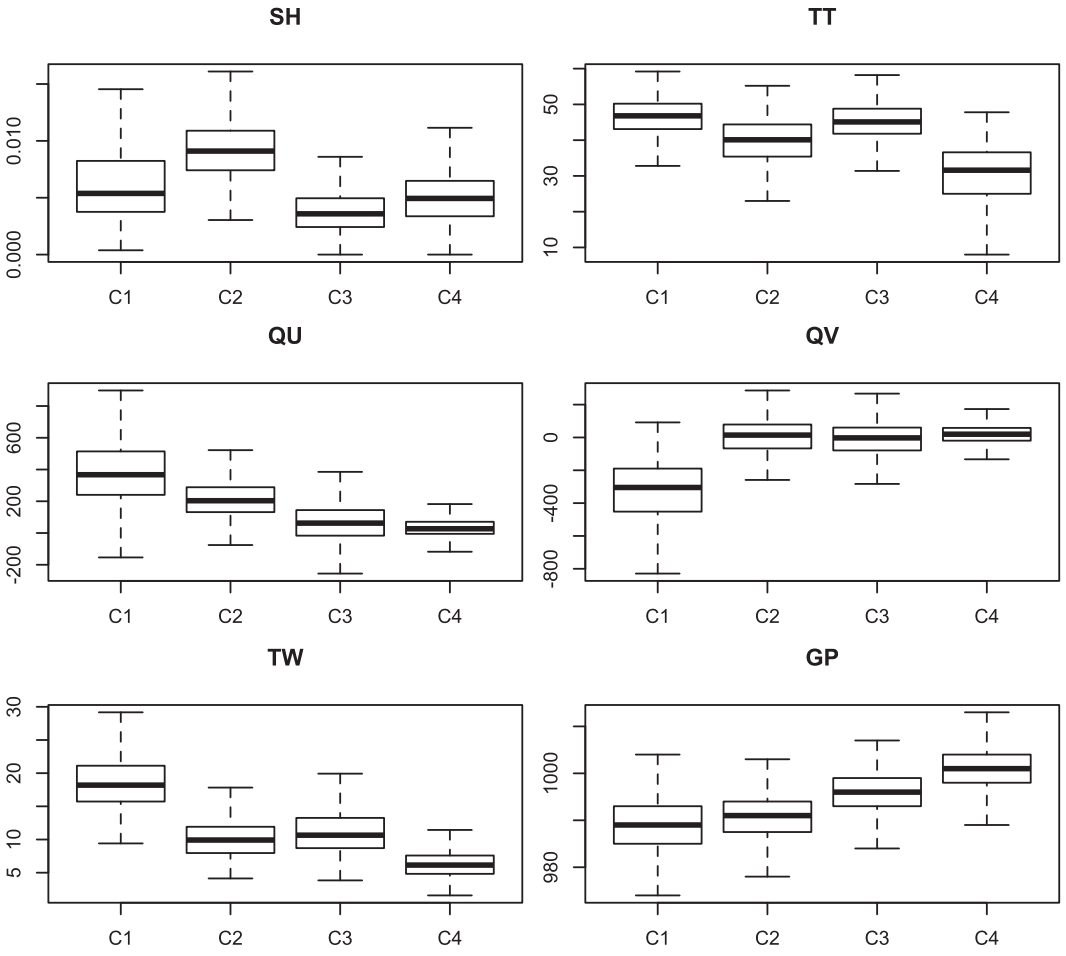

FIG. 4. Box plots of environmental variables for four clusters with outliers removed.

end of winter. The moderately dry class (C3) is most frequent at the start of winter (May and June), while the driest class (C4) is most likely to occur in midwinter (July and August). The interannual variability of the frequency of each class also varies along the 20-yr period. For example, the frequency of occurrence of the wettest classes (C1) varies from 4.4% in 1994 to 15.8% in 1995, with a 20-yr average of 10%.

It is useful to consider examples of the synoptic situations associated with each synoptic class in order to check the consistency of the deduced properties of each class. The days closest to the centers of C1–C4 are 24 October 1993, 25 June 2009, 5 August 1998, and 13 September 2000, respectively. The surface charts in Fig. 6 indicate that C1 and C2 tend to be associated with the passage of cold fronts, while C3 and C4 tend to be under the influence of high-pressure systems. The sounding for C1 shows moisture up to 300 hPa and strong westerly winds associated with a cold front. For C2 there is midlevel instability. Most of the moisture for C3 is below an inversion around 750 hPa, but there is an indication of upper-level cloud around 400 hPa. For C4, the sounding is very stable and dry.

5. Estimation of POP

The analysis of section 4 shows that a representation of the large-scale environment provided by soundings at Wagga Wagga can be used to associate each day

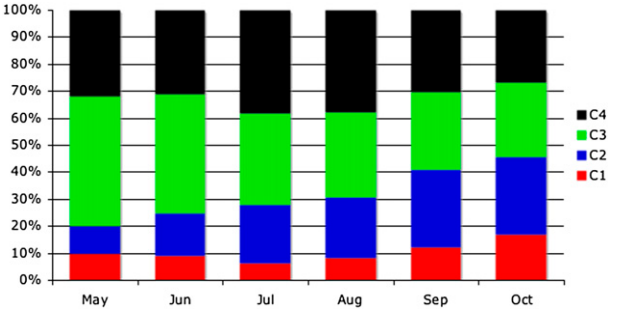

FIG. 5. Seasonal variability of synoptic classes (May–October, 1990–2009).

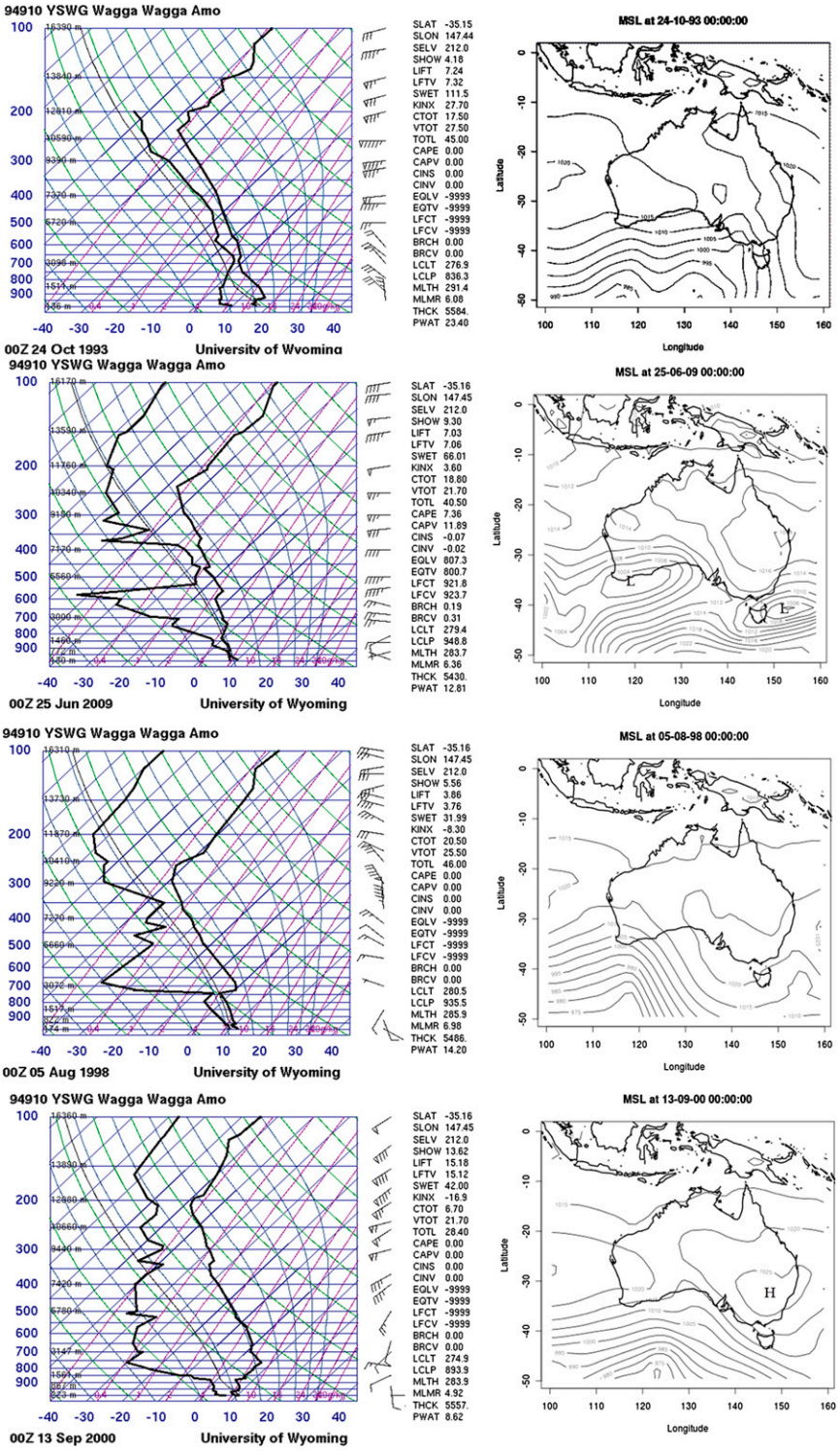

FIG. 6. Typical Wagga Wagga soundings and mean sea level charts for the four synoptic classes (from top to bottom) C1–C4.

TABLE 6. Performance of PME forecasts at day 1 over the period 2005–09. The first result is with a fixed value of 0.45 mm for the rain-day threshold, and the second result is with individual thresholds.

Synoptic classes (threshold)	Rain-days hit rate	No-rain-days false-alarm rate	RMS error on rain days (mm)	Bias on rain days (mm)	RMS error on no-rain days (mm)	Bias on no-rain days (mm)
C1 (0.80)	0.94, 0.97	0, 0	19.74, 20.37	12.34, 13.13	0.21, 0.78	−0.20, 0.11
C2 (0.40)	0.83, 0.81	0.39, 0.41	12.09, 12.50	7.58, 7.23	3.42, 3.47	1.40, 1.53
C3 (0.60)	0.79, 0.81	0.17, 0.21	7.67, 8.00	2.59, 2.76	1.08, 1.16	0.21, 0.22
C4 (0.35)	0.52, 0.48	0.20, 0.18	3.29, 2.91	0.45, 0.45	0.93, 2.91	0.23, 0.38

with one of four synoptic classes, with each class having a distinct precipitation distribution. It is therefore reasonable to ask whether the information associated with each class can be used to improve the PME precipitation forecasts. Two technical issues first need to be clarified.

We first note that the soundings are taken at 1000 LT on the day of the precipitation forecast, and so the forecast period overlaps with the input data. The use of earlier soundings is discussed in section 6, but at this stage we are simply considering whether the soundings early in the forecast period can be used to improve the PME forecast over the whole period.

A second technical issue is that the synoptic classification has been carried out over the period 1990–2009, while the PME data are available only for the period 2005–09. Comparing the precipitation in each period, we find that for 2005–09 it is similar to that for the 20-yr climatology. However, owing to the recent extended drought in southeastern Australia (Timbal 2009), Table 5 shows that the precipitation intensities are lower in the recent period, especially for class C4, where the intensity drops from 4.0 to 2.4 mm. We also find that the drier classes are more frequent than over the longer period; for example, the frequency of C4 increases from 21%–26%.

In section 3, we adjusted the threshold precipitation for all PME forecasts to obtain a bias score of 1.0 in the contingency table comparing observed and predicted rain days. That analysis has been repeated using the PME values for each of the four synoptic classes. The results are shown in Table 6; for the intensities, there is no significant difference in terms of RMS error and bias between the use of the fixed threshold of 0.45 mm and the use of individual thresholds for each cluster. For example, the rain-day hit rate for C1 is 0.94 with the fixed threshold and 0.97 with a threshold of 0.8 mm, to give a balanced contingency table for C1. Given the close similarity in the results for fixed and variable thresholds, we use the fixed value of 0.45 mm as the threshold between rain or no-rain threshold.

Comparing Table 6 with the values in Table 3 for day-1 forecasts, we see that the hit rate for rain days is improved for C1 and C2, while that for C3 is comparable with the overall hit rate. The low-precipitation class (C4) has a low hit rate, but the POP is only about 20% for this class. For C3 and C4, which make up about 70% of wintertime days, the no-rain false alarm rate is similar to that for all days (0.2). However, the no-rain false alarm rate for C2 is double the overall value, while the rate for C1 is reduced to zero; that is, all the uncertainty is accumulated in C2. The bias and RMS error on rain days tends to scale with the intensity for each class, as found in Table 3. On no-rain days the bias and RMS error tend to be less than in Table 3 for C3 and C4. On the other hand, the no-rain statistics for C2 are larger than in Table 3, while the errors in C1 are very small; that is, these statistics tend to scale with the false alarm rate for no-rain days.

6. Precipitation estimation

In section 5, we used the synoptic classification of section 4 to improve the identification of rain days and precipitation intensity on rain days from PME forecasts. We now consider whether the precipitation intensities on rain days can be improved by the application of a linear least squares fit between the PME and observed precipitation for each of the four synoptic classes.

As we found no significant difference between using individual thresholds for each class and the fixed threshold, we continue to use the fixed value of 0.45-mm as the rain-day threshold for PME forecasts. For the predicted rain days for each synoptic class, linear regression is applied to adjust the PME forecast for the region. In addition to the PME forecast, other variables with significant correlation (significance level of at least 5%) with the observed precipitation are used as predictors for the linear fit. GP is highly correlated for all four classes. QV is used as a predictor for C1. For C2 and C3, QU and TW are included. For C4, only GP and QU are applied.

To check the robustness of the regression analysis, we divide the 5-yr winter daily data into a control group and a test group. We use the control group to determine the coefficients for the linear regression, and then we calculate the RMS error for the test period to determine whether

TABLE 7. Results of regression analysis to adjust PME forecasts of rainfall intensity for each synoptic class.

Class	Predictors	RMS error (mm)	Adjusted PME RMS error (mm)
C1	PME, GP, QV	18.43	12.91
C2	PME, GP, TW, QU	11.78	9.35
C3	PME, GP, TW, QU	6.06	5.45
C4	PME, GP, QU	1.93	2.05

there is any improvement in the forecast of precipitation intensity compared with the basic PME. Around 60% of the data are assigned to the control group to get stable results. The earlier part of the data is used as control, and the later part is used for testing. In terms of RMS error in precipitation intensity, C1, C2, and C3 show an improvement in the forecast accuracy (see Table 7). The RMS error for C1 is reduced by more than 30%, dropping from 18 to 13 mm. However, the RMS error for the very dry class C4 is increased slightly from 1.9 to 2.1 mm. On the other hand, inspection of Table 6 shows that the RMS error in intensity from the basic PME is about 3 mm when data over the full period are used; that is, there is considerable uncertainty in the estimates for this very dry class. Furthermore, coefficient of determination (R^2) values for each predictor are calculated to examine the significance of each predictor. It is found that the PME is the most significant predictor for all four classes. For C1, it explains about 50% of the variation, while other predictors contribute only 7%. For C2, it explains around 33% compared with 10% of all other predictors.

A cross-validation experiment has been carried out to assess the robustness of these results. The linear regression has been repeated 10 000 times with random assignment of each day to either the control or test group. The range of RMS errors provides a measure of the uncertainty for each class. For C1, the median reduction in RMS error is 30%, with only a 3% chance of no improvement over the basic PME. For C2, there is a median decrease of 17% in RMS error, with an 8% chance of no improvement. The analysis, however, shows that the results for the two dry classes (C3 and C4) are not robust, with reductions in RMS error occurring only about 50% of the time. The lack of robustness is expected to be because of the small number of events in the dry classes; that is, a longer test period is needed to confirm these initial results.

7. Conclusions

The poor man's ensemble (PME) provides a useful forecast of daily precipitation across Australia. However, the estimation of wintertime precipitation in the Snowy Mountains is a challenge because of the lack of observations in the region, the occurrence of snow in high-wind conditions, and the relatively steep terrain in a small area. The availability of wintertime precipitation records at seven sites across the region allows for an independent assessment of the performance of the PME and for the development of a scheme to improve that performance.

It is found that the PME performs relatively well over the Snowy Mountains for some indicators. It has a hit rate of about 80% for rain days, with a false-alarm rate of about 20%. However, there are large errors in the estimation of precipitation intensity, with significant underestimation of precipitation in the mountains. The errors in the PME vary substantially from year to year, with the uncertainties tending to scale with the winter total precipitation.

Analysis of upper-air data from a site to the west of the Snowy Mountains shows that the precipitation can be classified into four distinct synoptic regimes. The classification is carried out using a cluster analysis based on six variables. It is found that the precipitation estimation errors vary with the synoptic weather regimes. Each synoptic class has a distinct precipitation distribution. Two of the classes (C1 and C2) are associated with wet conditions, and two (C3 and C4) are associated with drier conditions. C1 and C2 occur 30% of the time but contribute 70% of the wintertime precipitation. They tend to be associated with the passage of cold fronts from the west, while C3 and C4 tend to be associated with high-pressure systems.

For days falling into the very wet class (C1), the hit rate for rain from the PME increases from about 0.8 for all days to about 0.95; that is, the synoptic classification can be used to sharpen the reliability of the PME forecast of rain. A linear regression, using variables from the synoptic classification as well as the PME estimate, has been applied for each synoptic class to attempt to improve the prediction of precipitation intensity on rain days. It is found that the forecast RMS errors in intensity for the wet classes (C1 and C2) can be reduced by more than 20%. However, there are insufficient data to obtain statistically robust results for the two dry classes.

The present analysis is based on the sounding taken at the start of each day's precipitation, so its value for forecasting is limited. However, extension of the forecast period may be obtained by using predicted soundings from a numerical weather prediction model to estimate the synoptic regime for several days ahead.

Acknowledgments. We are grateful to Snowy Hydro Ltd. for providing the precipitation data for the Snowy

Mountains and for partial support for Jingru Dai, to the Australian Bureau of Meteorology for the PME data, and to Thomas Chubb for maps and advice.

REFERENCES

Abaurrea, J., and J. Asín, 2005: Forecasting local daily precipitation patterns in a climate change scenario. *Climate Res.,* **28,** 183–197, doi:10.3354/cr028183.

Bergant, K., and L. Kajfež-Bogataj, 2005: N–PLS regression as empirical downscaling tool in climate change studies. *Theor. Appl. Climatol.,* **81,** 11–23, doi:10.1007/s00704-004-0083-2.

Brunet, N., R. Verret, and N. Yacowar, 1988: An objective comparison of model output statistics and "perfect prog" in producing numerical weather element forecasts. *Wea. Forecasting,* **3,** 273–283, doi:10.1175/1520-0434(1988)003<0273:AOCOMO>2.0.CO;2.

Chubb, T. H., S. T. Siems, and M. J. Manton, 2011: On the decline of wintertime precipitation in the Snowy Mountains of south-eastern Australia. *J. Hydrometeor.,* **12,** 1483–1497, doi:10.1175/JHM-D-10-05021.1.

——, A. E. Morrison, S. Caine, S. T. Siems, and M. J. Manton, 2012: Case studies of orographic precipitation in the Brindabella Ranges: Model evaluation and prospects for cloud seeding. *Aust. Meteor. Oceanogr. J.,* **62,** 305–321. [Available online at http://www.bom.gov.au/amm/docs/2012/chubb.pdf.]

Ebert, E. E., 2001: Ability of a poor man's ensemble to predict the probability and distribution of precipitation. *Mon. Wea. Rev.,* **129,** 2461–2480, doi:10.1175/1520-0493(2001)129<2461:AOAPMS>2.0.CO;2; Corrigendum, **130,** 1661–1663, doi:10.1175/1520-0493(2002)130<1661:C>2.0.CO;2.

Enke, W., and A. Spekat, 1997: Downscaling climate model outputs into local and regional weather elements by classification and regression. *Climate Res.,* **8,** 195–207, doi:10.3354/cr008195.

Fowler, H., S. Blenkinsop, and C. Tebaldi, 2007: Linking climate change modeling to impacts studies: Recent advances in downscaling techniques for hydrological modeling. *Int. J. Climatol.,* **27,** 1547–1578, doi:10.1002/joc.1556.

Fraedrich, K., and L. M. Leslie, 1987: Evaluation of techniques for the operational, single station, short-term forecasting of rainfall at a midlatitude station (Melbourne). *Mon. Wea. Rev.,* **115,** 1645–1654, doi:10.1175/1520-0493(1987)115<1645:EOTFTO>2.0.CO;2.

Glahn, H. R., and D. A. Lowry, 1972: The use of model output statistics (MOS) in objective weather forecasting. *J. Appl. Meteor. Climatol,* **11,** 1203–1211, doi:10.1175/1520-0450(1972)011<1203:TUOMOS>2.0.CO;2.

Hartigan, J., and M. Wong, 1979: A K-means clustering algorithm. *J. Roy. Stat. Soc.,* **28C,** 100–108, doi:10.2307/2346830.

Henry, N. L., 2000: A static stability index for low-topped convection. *Wea. Forecasting,* **15,** 246–254, doi:10.1175/1520-0434(2000)015<0246:ASSIFL>2.0.CO;2.

Johnson, C. D., S. T. Siems, M. J. Manton, and E. E. Ebert, 2013: An evaluation of the precipitation forecasts of the Poor Man's Ensemble for wintertime rainfall across the southern portion of Australia. *Aust. Meteor. Oceanogr. J.,* **63,** 315–324. [Available online at www.bom.gov.au/amoj/docs/2013/johnson.pdf.]

Kent, D. M., D. G. C. Kirono, B. Timbal, and F. H. S. Chiew, 2013: Representation of the Australian sub-tropical ridge in the CMIP3 models. *Int. J. Climatol.,* **33,** 48–57, doi:10.1002/joc.3406.

Klein, W. H., and H. R. Glahn, 1974: Forecasting local weather by means of model output statistics. *Bull. Amer. Meteor. Soc.,* **55,** 1217–1227, doi:10.1175/1520-0477(1974)055<1217:FLWBMO>2.0.CO;2.

Larsen, S. H., and N. Nicholls, 2009: Southern Australian rainfall and the subtropical ridge: Variations, interrelationships, and trends. *Geophys. Res. Lett.,* **36,** L08708, doi:10.1029/2009GL037786.

Lorenz, E. N., 1969: Atmospheric predictability as revealed by naturally occurring analogues. *J. Atmos. Sci.,* **26,** 636–646, doi:10.1175/1520-0469(1969)26<636:APARBN>2.0.CO;2.

Marsaglia, G. W., W. Tsang, and J. Wang, 2003: Evaluating Kolmogorov's distribution. *J. Stat. Software,* **8.** [Available online at http://www.jstatsoft.org/v08/i18/.]

Morrison, A. E., S. T. Siems, and M. J. Manton, 2013: On a natural environment for glaciogenic cloud seeding. *J. Appl. Meteor. Climatol.,* **52,** 1097–1104, doi:10.1175/JAMC-D-12-0108.1.

Nicholls, N., 2010: Local and remote causes of the southern Australian autumn-winter rainfall decline, 1958–2007. *Climate Dyn.,* **34,** 835–845, doi:10.1007/s00382-009-0527-6.

Pook, M. J., P. C. McIntosh, and G. A. Meyers, 2006: The synoptic decomposition of cool-season rainfall in the southeastern Australian cropping region. *J. Appl. Meteor. Climatol.,* **45,** 1156–1170, doi:10.1175/JAM2394.1.

Raupach, M. R., P. R. Briggs, V. Haverd, E. A. King, M. Paget, and C. M. Trudinger, 2008: Australian Water Availability Project (AWAP). CSIRO Marine and Atmospheric Research Component, Final Rep. for Phase 3, 67 pp. [Available online at www.csiro.au/awap/doc/AWAP3.FinalReport.20080601.V10.pdf.]

Risbey, J. S., M. J. Pook, P. C. McIntosh, M. C. Wheeler, and H. H. Hendon, 2009: On the remote drivers of rainfall variability in Australia. *Mon. Wea. Rev.,* **137,** 3233–3253, doi:10.1175/2009MWR2861.1.

Saji, N. H., and T. Yamagata, 2003: Possible impacts of Indian Ocean dipole mode events on global climate. *Climate Res.,* **25,** 151–169, doi:10.3354/cr025151.

Smith, I. N., and B. Timbal, 2012: Links between tropical indices and southern Australian rainfall. *Int. J. Climatol.,* **32,** 33–40, doi:10.1002/joc.2251.

Timbal, B., 2009: The continuing decline in South-East Australian rainfall: Update to May 2009. CAWCR Research Letters, Issue 2, Bureau of Meteorology, Melbourne, Australia, 4–11. [Available online at www.cawcr.gov.au/publications/researchletters/CAWCR_Research_Letters_2.pdf.]

——, and W. Drosdowsky, 2013: The relationship between the decline of southeastern Australian rainfall and the strengthening of the subtropical ridge. *Int. J. Climatol.,* **33,** 1021–1034, doi:10.1002/joc.3492.

Wilson, L., M. J. Manton, and S. T. Siems, 2013: Relationship between rainfall and weather regimes in south-eastern Queensland, Australia. *Int. J. Climatol.,* **33,** 979–991, doi:10.1002/joc.3484.